

International Journal of Modern Physics A
© World Scientific Publishing Company

Perturbative study of large N principal chiral model with twisted reduction

Antonio González-Arroyo

*Instituto de Física Teórica UAM-CSIC, Nicolás Cabrera 13-15, Universidad Autónoma de Madrid, Cantoblanco, E-28049, Madrid, Spain;
Departamento de Física Teórica, Módulo 15, Universidad Autónoma de Madrid, Cantoblanco, E-28049, Madrid, Spain*

Ken-Ichi Ishikawa^{†*}, Yingbo Ji^{††} and Masanori Okawa[‡]

[†]*Core of Research for the Energetic Universe, Graduate School of Advanced Science and Engineering, Hiroshima University, Higashi-Hiroshima, Hiroshima 739-8526, Japan*

[‡]*Graduate School of Advanced Science and Engineering, Hiroshima University, Higashi-Hiroshima, Hiroshima 739-8526, Japan*

Received Day Month Year

Revised Day Month Year

We compute the first four perturbative coefficients of the internal energy for the twisted reduced principal chiral model (TRPCM) using numerical stochastic perturbation theory (NSPT). This matrix model has the same large N limit as the ordinary principal chiral model (PCM) at infinite volume. Indeed, we verify that the first three coefficients match the analytic result for the PCM coefficients at large N with a precision of three to four significant digits. The fourth coefficient also matches our own NSPT calculation of the corresponding PCM coefficient at large N . The finite- N corrections to all coefficients beyond the leading order are smaller for TRPCM than for PCM. We analyze the variance to determine the feasibility of extending the calculations to higher orders.

Keywords: Lattice Field Theory; Large N ; Perturbation Theory.

PACS numbers:11.10.-z,12.39.Fe,11.10.Ef,11.25.Db

1. Introduction

The two dimensional $SU(N) \times SU(N)$ principal chiral model (PCM) is often considered as a toy model for four-dimensional pure gauge theory, because they share many interesting properties,^{1–10} such as generating a mass gap¹¹ and being asymptotically free. To study these properties, various perturbative and non-perturbative methods have been applied. The large N expansion method can be applied to the

*Email ishikawa@theo.phys.sci.hiroshima-u.ac.jp

[†]Corresponding author, email d202186@hiroshima-u.ac.jp

2 *Antonio González-Arroyo, Ken-Ichi Ishikawa, Yingbo Ji, and Masanori Okawa*

PCM and gauge theories, where the standard weak-coupling expansion is reorganized to obtain better behavior and to simplify the Feynman diagrams to explain the perturbative properties of the theories. The lattice method has been applied to these models to study non-perturbative properties, and combining the lattice method with large N expansion is a natural way to understand their origin. Exploring the lattice PCM at large N is an important step toward the understanding of four-dimensional lattice gauge theories.

Our interest is in studying the high-order perturbative behavior of the lattice PCM at the large N limit. Motivated by the recently developed resurgence theory,^{12,13} one can deduce the non-perturbative effects, such as renormalon^{14,15} and the complex saddle point of the action, from the perturbation series in quantum field theory and quantum mechanics.¹⁶ To extract the non-perturbative effects from the perturbation series, we need to investigate the behavior of the coefficients in terms of the coupling g at rather high orders, such as $\mathcal{O}(g^{40}) - \mathcal{O}(g^{100})$. For models that are not analytically solvable, this is a difficult task without the help of numerical methods.

Numerical stochastic perturbation theory (NSPT) is a numerical method that can extract the perturbative coefficients at high orders semi-automatically.¹⁷ Recently, Bruckmann and Pühr have successfully extracted the renormalon behavior of the PCM from the high-order behavior of the perturbation coefficients of the internal energy.^{18,19} They computed the coefficients up to $\mathcal{O}(\lambda^{20})$, where λ is the 't Hooft coupling, for $N = 3-12$ on several lattice sizes up to 48^2 to extract the infinite-volume limits. The success of the high-order NSPT on the two-dimensional PCM in the large N limit might lead to a similar one for the four-dimensional large N gauge theories. However, applying the strategy of taking both the large N and infinite volume limits to the four-dimensional gauge theories could be computationally quite expensive. One approach to tackle the large N limit without taking the infinite volume limit is using the volume reduction method which has been first applied to the pure lattice gauge theory by Eguchi and Kawai.²⁰

Eguchi and Kawai showed that as $N \rightarrow \infty$ for the pure lattice gauge theory, the structure of the lattice could collapse into a single point provided that the Z_N symmetry is maintained, which led the Eguchi-Kawai-volume-reduced (EK) model. However, it has been realized that the original EK model does not reproduce the proper large N limit because of the spontaneous breaking of the Z_N symmetry in the continuum limit.²¹ Two of the present authors extended it to the twisted Eguchi-Kawai (TEK) model by introducing twisted boundary conditions, by which the internal degree of colour index is explicitly related to the degree of space-time lattice sites, and have shown that it realizes the correct continuum limit non-perturbatively.²²⁻²⁴ Twisted boundary conditions can be introduced for the PCM, and the corresponding twisted reduced principal chiral model (TRPCM) has been first investigated in Ref. 25. The large N limit of the TRPCM was later investigated in Ref. 26 non-perturbatively, where the choice of the flux value of the twisted boundary condition is extensively studied. By combining the TRPCM and

NSPT, we can study the high-order perturbation coefficients in the large N limit without taking explicitly infinite volume limit, as the large N limit involves implicitly taking the infinite volume limit. Another important property of the large N limit of the twisted reduced models is the realization of the master field property, a short simulation is enough to obtain the expectation values of observables, with the reduction of the variance through the factorization property in the large N limit. A study in this direction for the pure gauge theory has started in Ref. 27.

In this paper, we study the large N behavior of the perturbative coefficients of the internal energy for the TRPCM using NSPT. Before studying much higher orders in the large N limit, we first study the first fourth coefficients using NSPT. We examine the feasibility of a short NSPT simulation combined with the large N factorization and the master field property at a fixed but sufficiently large N . NSPT is a numerical application of the stochastic quantization method^{28,29} to the lattice models. Recently, it has a lot of achievements in many fields, including perturbative calculation in full and quenched QCD,^{30–32} high-order perturbative behavior^{18,19,33–35} always recognized as renormalon and even $g - 2$ in QED.³⁶ The original NSPT¹⁷ was based on the Langevin equation, and it has been extended to the hybrid molecular dynamics (HMD) based NSPT.^{32,37} We use the HMD-based NSPT for the TRPCM in this paper.

The present article is organized as follows. In Sec. 2 we will briefly review the cornerstone of our study, including reviews on the two dimensional $SU(N)$ TRPCM and the HMD-based NSPT algorithm. In Sec. 3 we present our numerical results obtained by applying NSPT to our model. We explore the N dependence of the first fourth-order coefficients of the internal energy. We also conduct a qualitative survey on the relation between N dependence of the variance and the statistical error through the factorization property, from which the number of independent samples required for a fixed statistical error is evaluated. In Sec. 4 we combine the results obtained in Sec. 3, the finite N corrections and the N dependence of the statistical error, to estimate the number of independent samples we need for performing high-order simulations at a single but sufficiently large N . Finally, a short summary is included in the last section.

2. Twisted reduced principal chiral model and numerical stochastic perturbation theory

In this section, we briefly describe the twisted reduced principal chiral model (TRPCM), and the numerical stochastic perturbation theory (NSPT) and its application to the TRPCM. We employ the hybrid molecular dynamics type NSPT algorithm including a randomized trajectory length scheme to circumvent the ergodicity problem in perturbation theory.

4 *Antonio González-Arroyo, Ken-Ichi Ishikawa, Yingbo Ji, and Masanori Okawa*

2.1. Review of TRPCM

The two dimensional $SU(N)$ twisted reduced principal chiral model (TRPCM)^{25,38} is specified by the following partition function:

$$\begin{aligned} Z &= \int dU \exp \{-S[U]\}, \\ S[U] &= bN \sum_{\mu=1,2} \text{Tr} (V_\mu V_\mu^\dagger), \\ V_\mu &\equiv \Gamma_\mu U \Gamma_\mu^\dagger - U, \end{aligned} \quad (1)$$

where U is a $SU(N)$ matrix, b is the inverse 't Hooft coupling defined as $b = 1/(Ng^2)$, and Γ_μ 's are the twist matrices. This model is deduced by the twisted volume reduction method from the lattice $SU(N) \times SU(N)/Z_N$ principal chiral model (PCM) with twisted boundary conditions.^{25,38} In the two dimensional case, the Γ_μ matrices satisfy 't Hooft algebra:²⁶

$$\Gamma_1 \Gamma_2 = \exp \left\{ i \frac{2\pi K}{N} \right\} \Gamma_2 \Gamma_1 \quad \Gamma_\mu \in SU(N). \quad (2)$$

For a given N and flux K , specific examples of two matrices, Γ_μ are provided by choosing a permutation matrix and a clock matrix according to the following equation respectively.

$$(\Gamma_1)_{i,j} = \delta_{\text{mod}(i, N) + 1, j}, \quad (3)$$

$$(\Gamma_2)_{i,j} = \delta_{i,j} \exp \left\{ i \frac{(2j - 1 - N)\pi K}{N} \right\}. \quad (4)$$

The TRPCM, Eq. (1), has the following global-symmetry:

$$U \rightarrow \Gamma(n) U \Gamma(n)^\dagger, \quad \Gamma(n) \equiv (\Gamma_1)^{n_1} (\Gamma_2)^{n_2}, \quad (n_1, n_2 = 0, \dots, N-1), \quad (5)$$

$$U \rightarrow UZ = ZU, \quad Z \in Z_N. \quad (6)$$

For large N , the planar sector of the TRPCM effectively corresponds to the lattice PCM defined on a square lattice with the size $L = N$. Therefore, as $N \rightarrow \infty$, the TRPCM meets both large N limit and infinite volume limit simultaneously, and eventually coincides with the PCM in both the large N and infinite volume limits.

The choice of K , the flux parameter, is important to realize the coincidence non-perturbatively in the large N and the continuum limit, and has been investigated in Refs. 24, 26, 27. For the equivalence in the large N limit, the center-symmetry (6) has to be maintained. Taking the large N limit with a constant K , the twist phase $\exp \left\{ \frac{2\pi i K}{N} \right\}$ in Eq. (2) might become ineffective to prevent the breaking of the center-symmetry.^{26,39,40} To avoid that, a feasible proposal of choosing the relation between K and N is given in Refs. 26, 40. For fixed N , K is chosen such that

$$\min_e e \left\| \frac{Ke}{N} \right\| > \Lambda, \quad (7)$$

where e runs over all integers co-prime with N , $\|\cdot\|$ is the distance to the nearest integer, and Λ is a threshold of $\Lambda \simeq 0.15$. We follow this choice in NSPT. It is also known that the twist phase is important for eliminating non-planar diagrams in the large N limit in perturbation theory, leading to smaller finite N corrections.

We employ the internal energy density operator E defined by

$$E = \frac{1}{2N} \sum_{\mu} \text{Re Tr} [U \Gamma_{\mu} U^{\dagger} \Gamma_{\mu}^{\dagger}], \quad (8)$$

as the main observable in this paper.

2.2. A brief introduction to NSPT for TRPCM

NSPT is a powerful tool for estimating high-order perturbative coefficients in quantum mechanics and lattice field theory. Since it builds on top of the stochastic quantization, the original NSPT is based on the Langevin equation.¹⁷ However, some limitations, including the lack of a high-order integrator to make the systematic error under control and the critical slow down in a critical situation, occur in the Langevin-based NSPT.

Because of the disadvantages of the Langevin-based NSPT, in this paper, we employ a hybrid molecular dynamics (HMD) based NSPT.^{41,42} The HMD method has been utilized to study a variety of complicated and non-local systems non-perturbatively and, in particular, its derivative hybrid Monte Carlo (HMC) has gained an important place in numerical computation and statistics. Applying the HMD to NSPT is a natural way to improve the efficiency of NSPT.¹⁷ A further improvement of NSPT beyond the HMD has been studied in Ref. 41.

To derive NSPT for the TRPCM more naturally, we first introduce the non-perturbative HMD simulation for the TRPCM as a starting point. The partition function for the HMD based Monte Carlo algorithm is translated from (1) as

$$Z = \int dU dP e^{-H[P,U]}, \quad (9)$$

$$H[P,U] = \frac{1}{2} \text{Tr} [P^2] + S[U]. \quad (10)$$

where P is a $N \times N$ traceless Hermitian matrix. The variable $\{P, U\}$ is stochastically generated to satisfy the probability density $dU dP e^{-H[P,U]}/Z$ in the HMD algorithm. The Markov chain for the density is constructed by regarding $H[P,U]$ as a Hamiltonian and introducing a fictitious time t for the dynamical variables $\{P, U\}$. The equation of motion for $\{P, U\}$ is

$$\frac{dU}{dt} = iPU, \quad \frac{dP}{dt} = F, \quad (11)$$

$$F = ibN \left(V - \frac{1}{N} \text{Tr} [V] \right), \quad V = UX - (UX)^{\dagger}, \quad (12)$$

$$X = \sum_{\mu} [\Gamma_{\mu}^{\dagger} U^{\dagger} \Gamma_{\mu} + \Gamma_{\mu} U^{\dagger} \Gamma_{\mu}^{\dagger}]. \quad (13)$$

6 *Antonio González-Arroyo, Ken-Ichi Ishikawa, Yingbo Ji, and Masanori Okawa*

The HMD algorithm uses a symplectic integration scheme to approximate the time evolution of the equation of motion, and the variable P is periodically refreshed as a stochastic variable from the Gaussian distribution $\exp[-\text{Tr}[P^2]/2]$. The Markov Chain Monte Carlo sampling of the HMD algorithm is used for the periodic sampling from the trajectory of $\{P, U\}$ as a function of time t .

NSPT formulation is obtained by replacing the variables $\{P, U\}$ in the EoM of the non-perturbative HMD (11) with their perturbative expansion in terms of the coupling constant. To take the large N limit of the TRPCM, the 't Hooft coupling $\lambda \equiv b^{-1}$ is a natural expansion parameter. The perturbative expansion for U and P is defined by

$$U = \sum_{k=0}^{\infty} \lambda^{k/2} U^{(k)}, \quad P = \lambda^{-1/2} \sum_{k=1}^{\infty} \lambda^{k/2} P^{(k)}, \quad (14)$$

where $U^{(0)} = I$ and $P^{(0)} = 0$ are imposed as the perturbative vacuum and non-dynamical variable. The first coefficient, $P^{(1)}$, is treated as the source of the randomness and generated from the Gaussian distribution $\exp[-\text{Tr}[(P^{(1)})^2]/2]$, while the higher order coefficients, $P^{(k)} (k > 1)$, are reset to zero at the beginning of each trajectory. As the force F starts at $\mathcal{O}(\lambda^{-1})$, we re-scale the expansion of P by $\lambda^{-1/2}$ and the unit of the fictitious time by

$$t = \lambda^{1/2} t', \quad (15)$$

to expand the EoM. We will omit $'$ for the re-scaled time unit hereafter.

The building blocks for the symplectic time integration scheme are

$$U^{(k)}(t + \delta t) = [e^{iP\delta t} \circledast U(t)]^{(k)}, \quad (16)$$

$$P^{(k)}(t + \delta t) = P^{(k)}(t) + F^{(k)}\delta t, \quad (17)$$

where δt is the discretized time step. The time of P in (16) and $F^{(k)}$ in (17) can be an arbitrarily time near t depending on the integration scheme in which they are involved. The symbol \circledast denotes the polynomial convolution product for two matrix polynomials. NSPT expansion for the matrix exponential $e^{iP\delta t}$ is given in Ref. 27. The perturbative expansion of the force F is derived as

$$F^{(k)} = iN \left(V^{(k)} - \frac{1}{N} \text{Tr}[V^{(k)}] \right), \quad V^{(k)} = S^{(k)} - S^{(k)\dagger}, \quad (18)$$

$$S^{(k)} = (U \circledast X)^{(k)}, \quad X^{(k)} = \sum_{\mu} \left[\Gamma_{\mu}^{\dagger} U^{(k)\dagger} \Gamma_{\mu} + \Gamma_{\mu} U^{(k)\dagger} \Gamma_{\mu}^{\dagger} \right]. \quad (19)$$

We also note that the HMD algorithm for NSPT possesses problems with non-ergodicity as discussed in Refs. 41–44. In order to keep it ergodic, two remedies have been established. One method is to systematically sample all Fourier mode of field variables by randomly varying the trajectory length t between samples. The alternative is to adjust the trajectory length to be shorter than a length below

which the HMD algorithm begins to resemble the original Langevin algorithm. In this study, we employ a method that combine these two approaches.

For the symplectic integrator for (16) and (17), we employ the 4th-order Omelyan–Mryglod–Folk (OMF) integrator,^{41,42} the finite integration error was expected to be proportional to δt^4 . The randomized trajectory length t_r is determined by

$$t_r = n_r \delta t, \quad \delta t = t/N_{md}, \quad (20)$$

where t is a fixed length, N_{md} is an integer for the number of time steps, and n_r is a random number generated as $n_r \leftarrow B(1/2, 2(N_{md} - 1)) + 1$ with the binomial distribution $B(p, n)$. Thus the averaged trajectory length is $\langle t_r \rangle = t$. All numerical results are computed at several δt values and extrapolated to $\delta t \rightarrow 0$ according to the δt^4 scaling before analyzing the N dependence.

The EoM is evolved for the randomized trajectory length and the perturbative coefficients $\{U^{(k)}, k = 1, \dots\}$, which are stochastic variables, are sampled as the Monte Carlo ensemble. The observables are also expanded perturbatively in λ , where the perturbative coefficients are the function of $\{U^{(k)}, k = 1, \dots\}$. The internal energy density operator E in Eq. (8) is expanded as

$$E = \sum_{k=0}^{\infty} \lambda^{k/2} E^{(k)}, \quad (21)$$

$$E^{(k)} = \frac{1}{2N} \sum_{\mu} \text{Re Tr} \left[(U \Gamma_{\mu} \otimes U^{\dagger} \Gamma_{\mu}^{\dagger})^{(k)} \right]. \quad (22)$$

The expectation value of the coefficient, $\langle E^{(k)} \rangle$, is evaluated as the statistical average on the ensemble for $\{U^{(k)}, k = 1, \dots\}$. The perturbation series is truncated in fixed order in the actual numerical simulation. In this paper, we keep the perturbation series up to λ^4 .

3. NSPT results

The numerical results of the TRPCM's perturbative coefficients which were described in the preceding section, are presented in this section. We determine that the PCM and the TRPCM have equivalent perturbative coefficients in the large N limit. We compare the first four perturbative coefficients of the internal energy of the TRPCM with NSPT to that of the PCM in the large N limit. Once these are shown, we confirm the reliability of our result using one of the important properties of large N limit - factorization, where we examine the variance of the coefficients converging to zero in the limit. Additionally, we estimate the number of independent samples at a fixed statistical error because the variance and the relative statistical error have a direct relation. In order to demonstrate the viability of the high-order computation with a single brief simulation at a sufficiently large but finite N , the finite N corrections and the estimation of the number of independent samples will be combined in the following section.

3.1. Numerical simulation and setup

We first discuss the numerical setup before diving into the components of the numerical results. As explained earlier, when choosing K parameter to perform the large N limit, there are several requirements. In Appendix A, we give the values of K that have been used.

We evaluate the perturbative coefficients of the internal energy and its variance up to $\mathcal{O}(g^8)$ or equivalently $\mathcal{O}(\lambda^4)$. The perturbative coefficients of the odd-order terms in g should be zero in perturbation theory. We have statistically confirmed this point within the one-sigma level in our numerical simulation. As a result, in the content that follows, we will only be concentrating on the perturbative coefficients of the even-orders of g .

The hyper-parameters of the NSPT simulation algorithm, the trajectory length t and the number of trajectory time step N_{md} , are tuned to satisfy the large N factorization property on the perturbative coefficients. This means that the variance of the perturbative coefficients vanishes in the large N limit. The details of the large- N factorization property on the variance are shown in Appendix B. We found that the trajectory length $t = 0.05$ is enough for the large N factorization for the first four order coefficients.

In this section, we show the results with the trajectory length at $t = 0.05$ using several N_{md} 's for the zero-step size limit. We accumulated over 2,000,000 trajectories after discarding the first 100,000 for thermalization. To remove the autocorrelation among the samples, we sample every trajectory and bin every 100 trajectories into a bin. Statistics are also shown in Tabs. 5–6 of Appendix A.

3.2. Internal energy

In the large N limit, the first three order results can be compared with the analytic formula for the PCM on an infinity volume lattice.^{45,46} Because there is no analytic formula, the fourth coefficient of the TRPCM cannot be directly compared. To have an insight into the large N limit of $\langle E^{(4)} \rangle$, we can employ the result from the NSPT simulation of PCM done by Bruckmann–Puhr,¹⁸ where the raw data are available in Ref. 47. We also perform another NSPT simulation with PCM because the Bruckmann–Puhr's data has fewer statistics to compare to our TRPCM result. Appendix C contains a detailed description of our NSPT simulation of PCM.

Fig. 1 is an example of the extrapolation to vanishing MD step size for the internal energy up to the fourth-order at $N = 21$. With our choice of the MD integrator, 4th order OMF, we linearly extrapolate with dt^4 . We found similar linear dependencies for the other N we investigated, removing the systematic error caused by the finite fictitious time step size. Following that, we will concentrate on the results at vanishing MD step size. Table 1 shows the perturbative coefficients of the internal energy at vanishing MD step size for each N .

Fig. 2 depicts the N dependence of the perturbative coefficient of the internal energy up to the fourth-order for all N data. The circles represent the TRPCM with

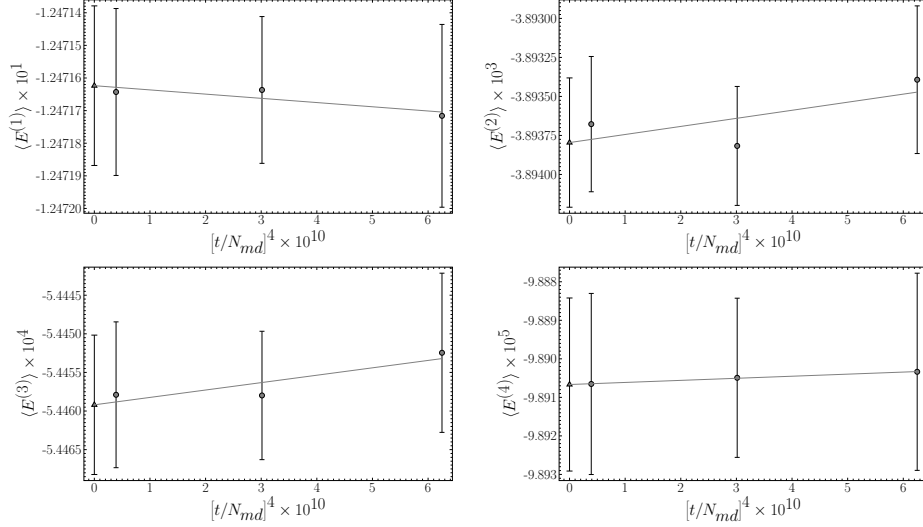
Perturbative study of large N principal chiral model with twisted reduction 9

Fig. 1. An overview of extrapolation to vanishing MD step size ($[t/N_{md}]^4 = \delta t^4 \rightarrow 0$). These plots show our numerical results obtained from $N = 21$ up to fourth order. The perturbative coefficients at $\delta t = 0$ are extracted with linear fitting in $[t/N_{md}]^4$.

Table 1. Perturbative coefficients for the internal energy after extrapolating to vanishing integration step size.

N	$\langle E^{(1)} \rangle$	$\langle E^{(2)} \rangle$	$\langle E^{(3)} \rangle$	$\langle E^{(4)} \rangle$
3	-0.111 122 34(1477)	-0.003 281 53(185)	-0.000 490 17(43)	-0.000 101 00(13)
5	-0.120 000 53(808)	-0.003 677 17(110)	-0.000 529 90(23)	-0.000 101 80(6)
7	-0.122 454 50(527)	-0.003 794 98(75)	-0.000 540 04(16)	-0.000 101 28(4)
9	-0.123 454 11(379)	-0.003 846 02(56)	-0.000 542 38(12)	-0.000 101 08(3)
11	-0.123 966 32(289)	-0.003 862 40(44)	-0.000 543 71(9)	-0.000 099 96(2)
13	-0.124 257 85(230)	-0.003 872 16(36)	-0.000 543 40(8)	-0.000 099 76(2)
15	-0.124 444 83(188)	-0.003 882 85(30)	-0.000 544 45(6)	-0.000 099 37(2)
17	-0.124 568 44(226)	-0.003 887 73(37)	-0.000 544 50(8)	-0.000 099 15(2)
19	-0.124 651 77(166)	-0.003 890 26(28)	-0.000 544 33(6)	-0.000 098 96(1)
21	-0.124 716 24(245)	-0.003 893 80(41)	-0.000 544 59(9)	-0.000 098 91(2)

NSPT results, and the solid curves present the analytic formula⁴⁵ for the PCM on an infinite volume lattice. The analytic values of the PCM coefficients up to the third order in an infinite volume are

$$\langle E^{(1)} \rangle = -\frac{N^2 - 1}{8N^2}, \quad (23)$$

$$\langle E^{(2)} \rangle = -\frac{N^2 - 1}{8N^2} \times \frac{N^2 - 2}{32N^2}, \quad (24)$$

$$\langle E^{(3)} \rangle = -\frac{N^2 - 1}{8N^2} \left[\frac{3N^4 - 14N^2 + 20}{768N^4} + \frac{N^4 - 4N^2 + 12}{64N^4} Q_1 + \frac{N^4 - 8N^2 + 24}{64N^4} Q_2 \right], \quad (25)$$

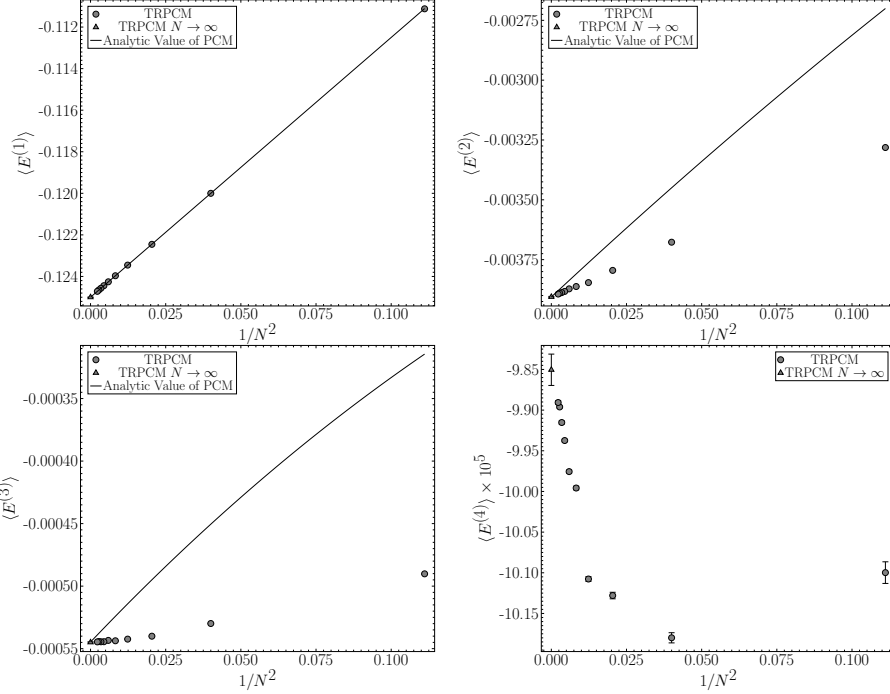
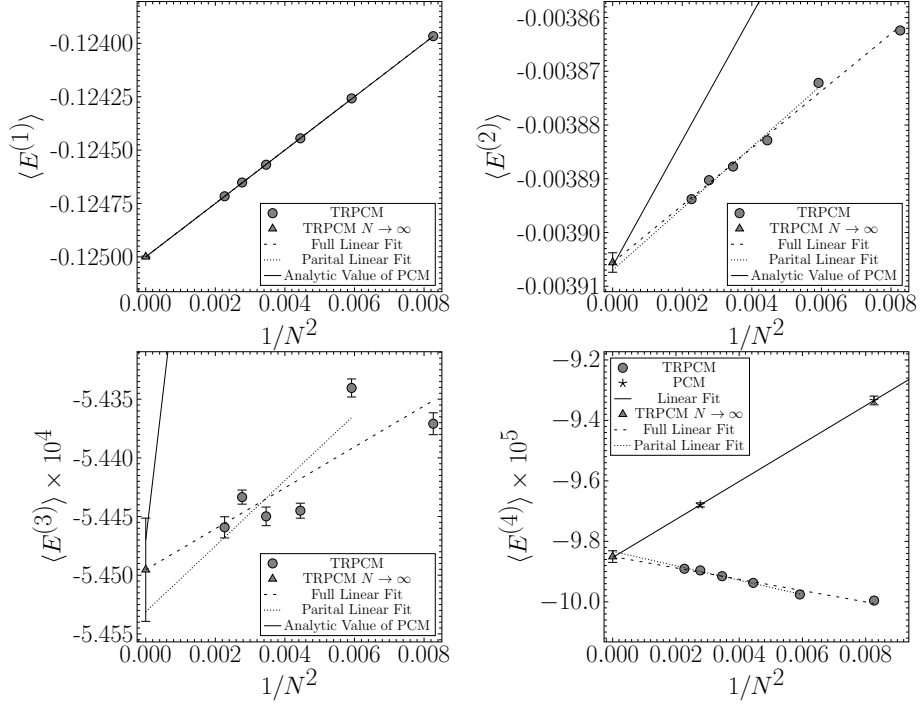
10 *Antonio González-Arroyo, Ken-Ichi Ishikawa, Yingbo Ji, and Masanori Okawa*

Fig. 2. N dependence of perturbative coefficients of the internal energy up to fourth order. The solid lines are plotted for Eqs. (23)–(25) as a function of $1/N^2$.

where $Q_1 = 0.0958876$ and $Q_2 = -0.0670$.⁴⁵ In Appendix D, we also provide the analytic values for the second order coefficient of the TRPCM for our values of N and K , demonstrating complete consistency of the NSPT results with them. Fig. 2 shows that the leading order results are identical to the PCM, whereas the second and third-order coefficients differ from the PCM at finite N . The N dependence of the TRPCM is milder than that of PCM indicating that the large N limit can be taken efficiently with the TRPCM. The effectiveness of the TRPCM is more enhanced by this smaller N dependence because the PCM needs double large limits on volume and N when taking the large N limit.

In the TRPCM, the N dependence corresponds to both finite N and finite volume corrections. We fit the NSPT data linearly in $1/N^2$ and the dashed and dotted lines represent the fit results as shown in Fig. 3. As we focus on the leading finite N correction, we fit data with $N \geq 11$. Dashed (dotted) lines show the fit with $N \geq 11$ ($N \geq 13$), respectively. The upper triangle at $N \rightarrow \infty$ corresponds to the extrapolation with the dashed fit and the error bar contains the statistical and systematic errors. The difference between the dotted and dashed fittings is used to calculate the systematic error. Table 2 shows the TRPCM's large N limit for the first four coefficients of the internal energy. The first three coefficients, $\langle E^{(k)} \rangle$, $k = 1, 2, 3$, are consistent with the analytic results of PCM in the large N limit.

Fig. 3. Magnification of Fig. 2 to show the limits as $N \rightarrow \infty$.Table 2. Comparison between analytic and NSPT results for $N \rightarrow \infty$. The first and second errors are the statistical error and the systematic errors from the fitting range, respectively.

Order i of $\langle E^{(i)} \rangle$	Analytic	NSPT
1	-0.125	-0.124 999 81(234)(83)
2	-0.003 906 25	-0.003 905 58(38) (143)
3	-0.000 544 70	-0.000 544 953(82)(358)
4	N.A.	-0.000 098 504(20)(172)

For the fourth-order coefficient, we compare the NSPT results between the PCM and TRPCM. We calculate the PCM coefficient at $N = 11$ and 19 at various volumes and use the infinite volume limit (for the details see Appendix C). The linear extrapolation on the PCM (solid line on stars in the bottom right panel of Fig. 3) is consistent with that of the TRPCM. We also note that the slope of the TRPCM is smaller than that of the PCM indicating the smallness of the finite N correction of the former.

Beyond the leading order, the finite N correction appears.⁴⁸ The linear fitting

12 *Antonio González-Arroyo, Ken-Ichi Ishikawa, Yingbo Ji, and Masanori Okawa*

results using $N \geq 11$ are

$$\langle E^{(1)} \rangle = -0.124\,999\,81(248) + \frac{0.125\,10(52)}{N^2}, \quad (26)$$

$$\langle E^{(2)} \rangle = -0.003\,905\,58(147) + \frac{0.005\,320(82)}{N^2}, \quad (27)$$

$$\langle E^{(3)} \rangle = -0.000\,544\,953(367) + \frac{0.000\,174(17)}{N^2}, \quad (28)$$

$$\langle E^{(4)} \rangle = -0.000\,098\,504(173) + \frac{-0.000\,187\,4(42)}{N^2}. \quad (29)$$

The coefficients of $\mathcal{O}(1/N^2)$ term for $\langle E^{(2)} \rangle$ and $\langle E^{(3)} \rangle$ are smaller than those of PCM ($3/256 \simeq 0.01171875$ for $\langle E^{(2)} \rangle$ and 0.002525595 for $\langle E^{(3)} \rangle$).

We also noted that, for each order of perturbation, the magnitude of the coefficient of the $1/N^2$ term has the same order as that of the constant term. By performing a single simulation at a finite but sufficiently large N , where N is determined by requiring that the magnitude of the finite N correction is smaller than that of the statistical error, we can safely evaluate the coefficients at the large N limit. As we will see in the following subsection, the variance and the large N factorization can both have an impact on the relative magnitude of the statistical error with the finite N correction. In this way, we can estimate the number of statistical samples required to get a statistical error exceeding the finite N correction of a single large value of N . This issue will be covered in section 4.

3.3. Large N factorization and statistical error

Using NSPT, we were able to obtain appropriate fit lines in the previous subsection that provided consistent values for the large N limit for the first four order coefficients. In order to see the confidence in the large N limit, we also validate another important property of large N field theory called large N factorization.^{49,50}

According to the large N factorization, the expectation value of the product of single trace local operators at different sites becomes the product of each expectation value of the local operators. The finite N correction to the factorization scales as a function $f(1/N) \rightarrow 0$ in $N \rightarrow \infty$. This property can be checked by observing the statistical variance of a local operator in the TRPCM as it corresponds to the finite N correction as seen below.

The statistical error is proportional to the square root of the variance and inversely proportional to the number of independent samples of the Markov chain Monte Carlo simulation. The large N factorization property leads to a decrease of the variance with N implying also a reduction in the number of statistical samples needed to achieve a certain precision with NSPT for the perturbative coefficients of the internal energy.

The factorization property indicates that the variance of the internal energy,

Table 3. Variance of perturbative coefficients of the internal energy after extrapolating to vanishing integration step size.

N	$\text{Var}[E^{(1)}] \times 10^4$	$\text{Var}[E^{(2)}] \times 10^6$	$\text{Var}[E^{(3)}] \times 10^7$	$\text{Var}[E^{(4)}] \times 10^8$
3	0.2312(10)	0.3639(17)	0.1941(12)	0.1874(19)
5	0.069 19(30)	0.127 63(56)	0.058 45(27)	0.041 53(22)
7	0.029 38(12)	0.060 03(26)	0.026 70(11)	0.017 085(79)
9	0.015 236(66)	0.033 74(14)	0.014 971(65)	0.009 203(41)
11	0.008 863(38)	0.020 659(90)	0.009 228(40)	0.005 554(24)
13	0.005 601(24)	0.013 890(61)	0.006 247(27)	0.003 741(17)
15	0.003 789(16)	0.009 662(42)	0.004 364(18)	0.002 578(11)
17	0.002 705(14)	0.007 339(39)	0.003 375(18)	0.002 047(11)
19	0.001 981(95)	0.005 496(26)	0.002 575(12)	0.001 571 2(75)
21	0.001 510(12)	0.004 325(33)	0.002 064(15)	0.001 271 7(99)

$\text{Var}[E]$, should behave as

$$\text{Var}[E] = \langle E^2 \rangle - \langle E \rangle^2 \xrightarrow{N \rightarrow \infty} 0. \quad (30)$$

The same factorization property holds for each perturbation coefficient $\langle E^{(k)} \rangle$. As one of the validations of the outcomes assessed with NSPT, we use this property to examine the variance of the internal energy in each order by fitting the $1/N^2$ dependence.

Fig. 4 and Table 3 depict the N dependence of the variance. Fig. 5 is the magnification of Fig. 4 for the large N limit. We fit the variance as a linear function of $1/N^2$ as

$$\text{Var}(E^{(k)}) = \text{Var}(E^{(k)})_{N \rightarrow \infty} + \frac{a^{(k)}}{N^2}. \quad (31)$$

The dashed and dotted lines are fit results with and without $N = 11$ data, respectively. We clearly observe the vanishing variance in the $N \rightarrow \infty$ limit. The up-triangles at $1/N^2 = 0$ are the results without $N = 11$ data and the error includes statistical and systematic errors assigned with the discrepancy between the two fit results. Table 4 shows the fit results. The fitting results for $\text{Var}(E^{(k)})_{N \rightarrow \infty}$ are consistent with zero where the first and the second errors are the statistical and the systematic errors, respectively. This shows that our simulation setup effectively maintains the large N factorization property. In light of this, these results provide a precise cross-check for the reliability of our NSPT results up to the fourth-order. Additionally, we see that as order k increases, the slope $a^{(k)}$, where we only mention the statistical error, decreases.

The statistical error is related to the variance and the number of statistical sample as

$$\left(\delta E^{(k)} \right)^2 = \frac{\text{Var}(E^{(k)})}{N_{\text{sample}}}, \quad (32)$$

where $\delta E^{(k)}$ is the statistical error of $\langle E^{(k)} \rangle$.

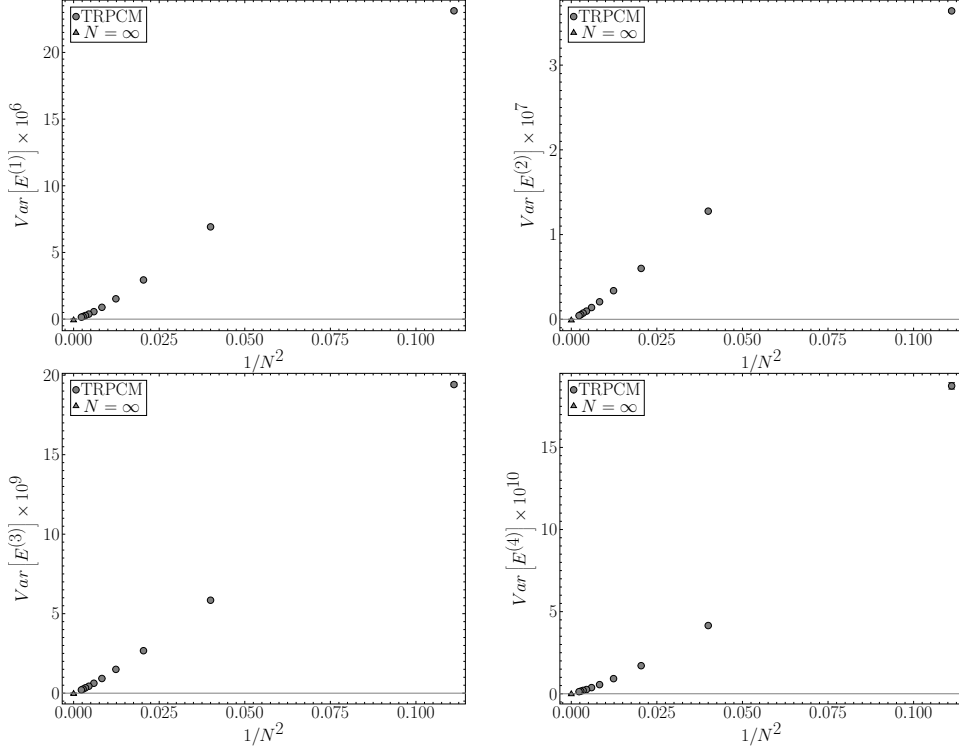


Fig. 4. The N dependence of variance of perturbative coefficients of the internal energy up to fourth order.

Table 4. Variance of internal energy after performing the extrapolation to infinite N .

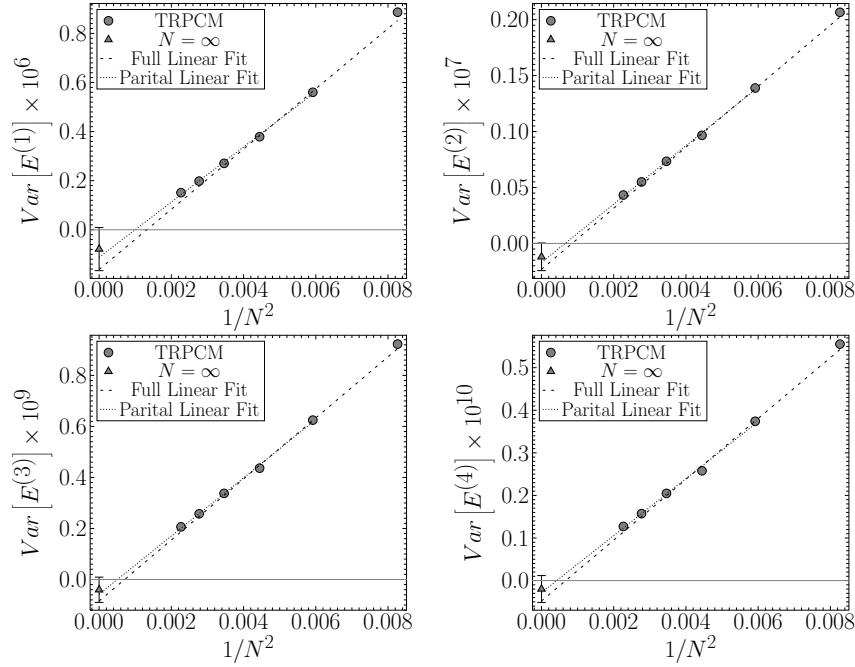
Order i of $\text{Var}[E^{(i)}]$	$\text{Var}[E^{(i)}]_{N \rightarrow \infty}$	$a^{(i)}$
1	$-0.786(45)(834) \times 10^{-7}$	$0.11242(68) \times 10^{-3}$
2	$-0.119(11)(111) \times 10^{-8}$	$0.2612(17) \times 10^{-5}$
3	$-0.403(54)(440) \times 10^{-10}$	$0.11403(78) \times 10^{-6}$
4	$-0.198(33)(282) \times 10^{-11}$	$0.6693(47) \times 10^{-8}$

The number of the statistical samples needed for a fixed relative statistical error can be estimated as

$$N_{\text{sample}} = \frac{\text{Var}(E^{(k)})}{\langle E^{(k)} \rangle^2} \left(\frac{\langle E^{(k)} \rangle}{\delta E^{(k)}} \right)^2. \quad (33)$$

In the large N limit, $\text{Var}(E^{(k)})$ and $\langle E^{(k)} \rangle$ behave as

$$\text{Var}(E^{(k)}) \simeq \frac{a^{(k)}}{N^2}, \quad \langle E^{(k)} \rangle \simeq \langle E^{(k)} \rangle_{\infty} + \frac{b^{(k)}}{N^2}. \quad (34)$$

Fig. 5. Magnification of Fig. 4 to show the limits as $N \rightarrow \infty$.

For a fixed relative statistical error, the number of statistical samples scales as

$$N_{\text{sample}} \simeq \frac{1}{N^2} \frac{a^{(k)}}{\langle E^{(k)} \rangle_\infty^2} \left(\frac{\langle E^{(k)} \rangle}{\delta E^{(k)}} \right)^2, \quad (35)$$

in the large N limit. For a fixed relative error, the number of statistical samples decreases as $1/N^2$ for the large N limit. This is just the so-called master field property of the large N limit.⁵¹ Conversely, the relative statistical error decreases as increasing N linearly at a fixed number of samples as

$$\frac{\delta E^{(k)}}{|\langle E^{(k)} \rangle|} = \frac{\sqrt{\text{Var}(E^{(k)})}}{\sqrt{N_{\text{sample}}}} \simeq \frac{\sqrt{a^{(k)}}}{N \sqrt{N_{\text{sample}}}}. \quad (36)$$

In the previous subsection, we investigated the finite N correction for $\langle E^{(k)} \rangle$. The size of N with which the finite N correction is sufficiently smaller than the statistical error can be estimated. In order to estimate the number of statistics with a single simulation for the large N limit, we will combine the property of the finite N correction and the N dependence of the relative statistical error in the following section.

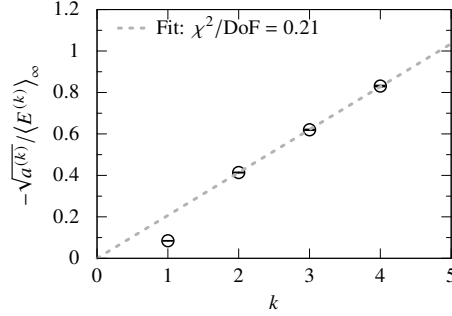


Fig. 6. The k dependence of $-\sqrt{a^{(k)}}/\langle E^{(k)} \rangle_\infty$.

4. Outlook

The large N results of the TRPCM will be performed in a single simulation as our ultimate objective. With a fixed number of statistical samples, as shown in Eq. (36), the relative statistical error decreases toward the large N limit. When the magnitude of the finite N correction term $|b^{(k)}|/N^2$ is comparable to the statistical error of the coefficient $\langle E^{(k)} \rangle_\infty$, we can recognize the value of $\langle E^{(k)} \rangle$ at the finite N as the value at the large N limit. This means that we could obtain the large N result of the TRPCM with a single simulation without large N extrapolation if the statistical error and the N correction occur in the same order at a sufficiently large but finite N . We explore this possibility as our outlook for the high-order NSPT calculation of the TRPCM at the large N limit.

To do this, we have to estimate the k dependence of the finite N corrections, $a^{(k)}$ and $b^{(k)}$, larger than 4. We fit the ratio $-\sqrt{a^{(k)}}/\langle E^{(k)} \rangle_\infty$ as a function of order k using the data at $k > 1$. We show our fitting results in Fig. 6. It shows a linear behavior as

$$\frac{\sqrt{a^{(k)}}}{|\langle E^{(k)} \rangle_\infty|} = 0.207k. \quad (37)$$

For the finite N correction term, $|b^{(k)}|/(N^2 \langle E^{(k)} \rangle)$, our observation based on Eqs. (26)–(29) suggests $|b^{(k)}| \sim |\langle E^{(k)} \rangle|$ so that the finite N correction behaves as $1/N^2$. The Feynman diagrammatic argument, however, suggests the finite N correction may increase as k rises. In light of this, we, now, consider two possible functional forms for the finite N correction.

$$\left| \frac{b^{(k)}}{\langle E^{(k)} \rangle_\infty} \right| = 1 \quad \text{or} \quad \left| \frac{b^{(k)}}{\langle E^{(k)} \rangle_\infty} \right| = k. \quad (38)$$

Now we analyze the feasibility of a single simulation at a large but finite N for extracting the perturbation coefficients in the large N limit at a higher order. We set the desired order to be $k = 20$, which order enables us to observe the renormalon

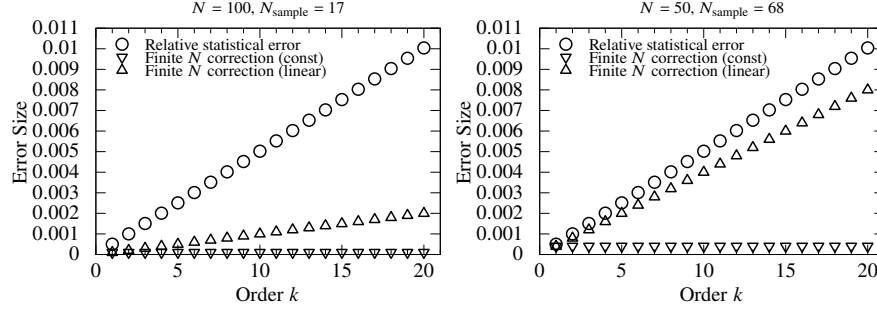


Fig. 7. The k dependence of relative statistical error and finite N correction. The number of independent samples is determined by fixing the relative statistical error to be 1% at order $k = 20$.

behavior as in Ref. 18, and the relative error as $\delta E^{(k=20)} / |\langle E^{(k=20)} \rangle| = 1\%$. We also fix the size of N to be 100 for example.

Using Eq. (35), we obtain the number of samples needed to reach a relative statistical error for an order k as

$$N_{\text{sample}} \simeq \left(\frac{0.207k}{N} \right)^2 \left(\frac{\langle E^{(k)} \rangle}{\delta E^{(k)}} \right)^2. \quad (39)$$

Substituting the settings, $k = 20$ and $\delta E^{(k=20)} / |\langle E^{(k=20)} \rangle| = 1\%$ into this equation, we obtain $N_{\text{sample}} = 17$. With $N_{\text{sample}} = 17$, we investigate the possibility that the finite N correction is comparable to or smaller than the statistical error at each order lower than $k = 20$. The left panel in Fig. 7 shows the k dependence of the relative statistical error and finite N correction with $N = 100$. The circles are the relative statistical error with $N_{\text{sample}} = 17$, which is determined as 1% at $k = 20$. The up and low triangles are the finite N correction with constant and linear assumptions (38), respectively. Both of the finite N corrections are sufficiently smaller than the statistical error so that the single simulation at $N = 100$ with $N_{\text{sample}} = 17$ effectively yields the perturbative coefficients up to the 20th order in the large N limit.

On the other hand, the finite N correction increases for smaller N , making it statistically visible. The right panel in Fig. 7 shows the k dependence of the relative statistical error and finite N correction with $N = 50$, where $N_{\text{sample}} = 68$ is determined in the same manner to $N = 100$. The finite N correction with linear dependence approaches the statistical error. Below $N = 50$, the finite N correction could be statistically visible with the linear dependence assumption.

As was mentioned above, setting the relative statistical error at a higher order coefficient and making the assumption that the finite N corrections depend on k , the large N limit could be reached with a single NSPT simulation at a large enough N value.

5. Summary

In this study, we have applied NSPT to the TRPCM and evaluated the perturbative coefficients of the internal energy up to $\mathcal{O}(g^8)$ or equivalently $\mathcal{O}(\lambda^4)$. We have shown that at the large N limit the first three order coefficients agree exactly with the analytic results of the lattice PCM on an infinite volume lattice. With the help of an independent NSPT simulation of the lattice PCM, we were able to accurately extract the fourth-order coefficient in the large N limit. We discussed the possibility of $N = \infty$ limit simulation with a single NSPT simulation at a sufficiently large but finite N value from the consistent large N factorization property of the observable. We investigated whether the $N = \infty$ simulation could be successfully carried out $N = 100$ with a 1% relative statistical error at the 20th order coefficient, where the finite N corrections could be statistically invisible under the assumption that they depend only on the order of the perturbation, rather than having a more complex dependence. To demonstrate the benefit of the TRPCM that the large N and large volume limits are taken effectively with a single simulation, more NSPT simulation at larger N and higher order should be run.

6. Acknowledgments

We thank Falk Bruckmann for pointing us the location of the raw data of their PCM work. A.G.-A. is partially supported by grant PGC2018-094857-B-I00 funded by MCIN/AEI/ 10.13039/501100011033 and by “ERDF A way of making Europe”, and by the Spanish Research Agency (Agencia Estatal de Investigación) through grants IFT Centro de Excelencia Severo Ochoa SEV-2016-0597 and No CEX2020-001007-S, funded by MCIN/AEI/10.13039/501100011033. He also acknowledges support from the project H2020-MSCAITN-2018-813942 (EuroPLEx) and the EU Horizon 2020 research and innovation programme, STRONG-2020 project, under grant agreement No 824093. K.-I.I. is supported by MEXT as “Program for Promoting Researches on the Supercomputer Fugaku” (Simulation for basic science: from fundamental laws of particles to creation of nuclei, JPMXP1020200105) and JICFuS. M.O. is supported by JSPS KAKENHI Grant Number 21K03576. The computation was carried out using the computer resource offered under the category of General Projects by Research Institute for Information Technology, Kyushu University.

Appendix A. Numerical parameters

This appendix contains a detailed description of the specifics of the numerical parameters. It also includes the NSPT parameters for the models that we are studying, as shown in Tables 5–6. To take the smooth large N limit of the TRPCM, we keep $\frac{\bar{K}}{N}$ about a constant which is 0.38. For the NSPT, we show various trajectory lengths t and N_{md} . Furthermore, we show the number of statistical samples. The number

Table 5. Simulation parameters and statistics for $N = 3$ –13

N	$\left(\frac{L}{a}\right)^2$	K	\bar{K}	$\frac{\bar{K}}{N}$	t	$(N_{md}, \text{Statistics})$
3	9	1	1	0.33	0.05	(10, 10 000 000) (12, 10 000 000) (20, 10 000 000)
5	25	3	2	0.4	0.05	(10, 10 000 000) (12, 10 000 000) (20, 10 000 000)
7	49	5	3	0.43	0.05	(10, 10 000 000) (12, 10 000 000) (20, 10 000 000)
9	81	7	4	0.44	0.05	(10, 10 000 000) (12, 10 000 000) (20, 10 000 000)
11	121	3	4	0.36	0.025	(5, 1 000 000) (6, 1 000 000) (10, 1 000 000)
					0.05	(10, 10 000 000) (12, 10 000 000) (20, 10 000 000)
					0.08	(16, 1 000 000) (19, 1 000 000) (32, 1 000 000)
					0.1	(20, 1 000 000) (24, 1 000 000) (40, 1 000 000)
					0.2	(40, 500 000) (48, 500 000) (80, 500 000)
					0.5	(100, 500 000) (120, 500 000) (200, 500 000)
13	169	8	5	0.38	0.025	(5, 1 000 000) (6, 1 000 000) (10, 1 000 000)
					0.05	(10, 10 000 000) (12, 10 000 000) (20, 10 000 000)
					0.08	(16, 1 000 000) (19, 1 000 000) (32, 1 000 000)
					0.1	(20, 1 000 000) (24, 1 000 000) (40, 900 000)
					0.2	(40, 500 000) (48, 500 000) (80, 500 000)
					0.5	(100, 800 000) (120, 600 000) (200, 500 000)

of independent samples can be obtained from the following equation

$$N_{independent} = \frac{N_{Statistics}}{N_{bin}}, \quad (\text{A.1})$$

where, in our case, N_{bin} is assigned as 100.

Appendix B. Hyper-parameters

This appendix contains a description of the analysis of the NSPT simulation's hyper-parameters. The length of trajectory (t) and the number of MD steps (N_{md}) for the trajectory of the MD evolution serve as the hyper-parameters in this study. As described in the main text, the large N factorization property is a metric for a suitable choice of the hyper-parameters. We note that the HMD algorithm for NSPT could possess non-ergodicity as discussed in Refs. 41–44. To ensure the ergodicity, we investigate the large N factorization property using the vanishing variance in the large N limit.

We investigate the t dependence of the variance of perturbative coefficients evaluated at $t = 0.5, 0.2, 0.1, 0.08, 0.05, 0.025$ for $11 \leq N \leq 19$. The finite time step size error is removed by extrapolating $\delta t \rightarrow 0$ using data at three N_{md} 's at each t as shown in table 5.

Fig. 8 shows the N dependence of the variance of the leading order coefficient for

20 *Antonio González-Arroyo, Ken-Ichi Ishikawa, Yingbo Ji, and Masanori Okawa*Table 6. Same as table 5, but for for $N = 15\text{--}21$

N	$\left(\frac{L}{a}\right)^2$	K	\bar{K}	$\frac{\bar{K}}{N}$	t	$(N_{md}, \text{Statistics})$
15	225	4	4	0.27	0.025	(5, 1 000 000) (6, 1 000 000) (10, 1 000 000)
					0.05	(10, 10 000 000) (12, 11 000 000) (20, 10 000 000)
					0.08	(16, 1 000 000) (19, 1 000 000) (32, 1 000 000)
					0.1	(20, 6 000 000) (24, 3 000 000) (40, 3 000 000)
					0.2	(40, 500 000) (48, 500 000) (80, 500 000)
					0.5	(100, 600 000) (120, 550 000) (200, 500 000)
17	289	5	7	0.41	0.025	(5, 1 000 000) (6, 1 000 000) (10, 1 000 000)
					0.05	(10, 7 240 200) (12, 7 944 400) (20, 4 684 000)
					0.08	(16, 1 000 000) (19, 1 000 000) (32, 1 000 000)
					0.1	(20, 5 000 000) (24, 5 000 000) (40, 4 000 000)
					0.2	(40, 500 000) (48, 500 000) (80, 500 000)
					0.5	(100, 800 000) (120, 800 000) (200, 600 000)
19	361	11	7	0.37	0.025	(5, 1 000 000) (6, 1 000 000) (10, 1 000 000)
					0.05	(10, 9 000 000) (12, 8 435 100) (20, 6 435 800)
					0.08	(16, 1 000 000) (19, 1 000 000) (32, 1 000 000)
					0.1	(20, 1 900 000) (24, 2 200 000) (40, 1 100 000)
					0.2	(40, 800 000) (48, 500 000) (80, 500 000)
					0.5	(100, 1 010 000) (120, 1 010 000) (200, 550 000)
21	441	8	8	0.38	0.05	(10, 2 036 200) (12, 3 084 400) (20, 2 411 300)

each t . The dashed and dotted lines show the linear fit in $1/N^2$ on the data with and without $N = 11$, respectively. The errors as $N \rightarrow \infty$ include the statistical error and systematic error assigned by fittings with and without the data at $N = 11$. Although the variances are small in $\mathcal{O}(10^{-6})\text{--}\mathcal{O}(10^{-7})$, those for $t > 0.08$ show a non-smooth behavior. While those for $t \leq 0.08$ show a smooth linear dependence resulting in the factorization property in the large N limit. Fig. 9 shows those for the fourth order coefficient for each t . Similarly to Fig. 8, the variances for $t \leq 0.08$ show a smooth linear dependence in the large N limit. The large N factorization property is met, so our choice of $t = 0.05$ is valid even though the reason for the irregular behavior in longer mean trajectory length $t > 0.08$ is not fully understood in this study.

Appendix C. Fourth order coefficients of PCM

The results of the lattice PCM's fourth-order coefficients evaluated with NSPT are included in this appendix. Bruckmann and Puhr have been evaluated the coefficient of PCM up to $\mathcal{O}(\lambda^{20})$ ¹⁸ and their raw data are available in Ref. 47. We perform

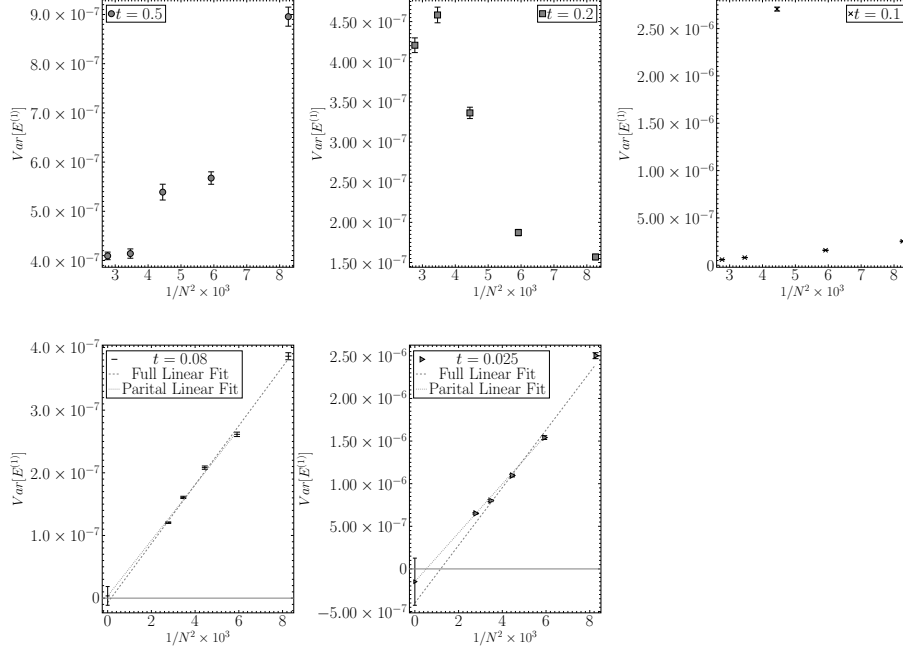
Perturbative study of large N principal chiral model with twisted reduction 21

Fig. 8. The hyper-parameter dependency of variance of internal energy at the leading order case. For $t = 0.08$ and 0.025 data, linear fit in $1/N^2$ is applied. The errors as $N \rightarrow \infty$ include the statistical error and systematic error assigned by fittings with and with out of the data at $N = 11$.

an additional NSPT simulation for the PCM with higher statistics than that of Refs. 18,47 in order to compare the PCM and the TRPCM at a comparable statistical error level for the first four order coefficients. In the range of $L = 12 - 48$ for the lattice size, we use nine different sizes with periodic boundary conditions within the PCM. We use the 4th order OMF integrator with the HMD-based NSPT lacking a randomly generated trajectory length. We fix the trajectory length at $t = 0.05$ and use several time steps to take the vanishing δt limit. We added a global chiral symmetry breaking term to the MD equation, similar to the gauge fixing term and reunitarization process to stabilize the MD trajectory. We accumulated 100 000 trajectories for each simulation parameter, and computed the perturbation coefficients at $N = 11$ and 19 . The statistical errors are estimated using the single eliminated jackknife method after binning every 1000 trajectories. After taking $\delta t \rightarrow 0$ limit with $\mathcal{O}(\delta t^4)$ scaling, the infinite volume limit is taken with the RG-based method as described in Ref. 18. We include the perturbative beta function in the lattice scheme up to third order⁴⁵ and a linear term of $1/L^4$ in the RG-based fit function.

Table 7 contains the coefficients for the first forth orders with the PCM at various lattice sizes L . The $L \rightarrow \infty$ limit of $\langle E^{(4)} \rangle$ is extracted with the simultaneous fit using the RG-based volume dependence model with the constraint on the analytic values for $\langle E^{(k=1,2,3)} \rangle$ of the PCM in the $L \rightarrow \infty$ limit. Figs. 10 and 11 show the

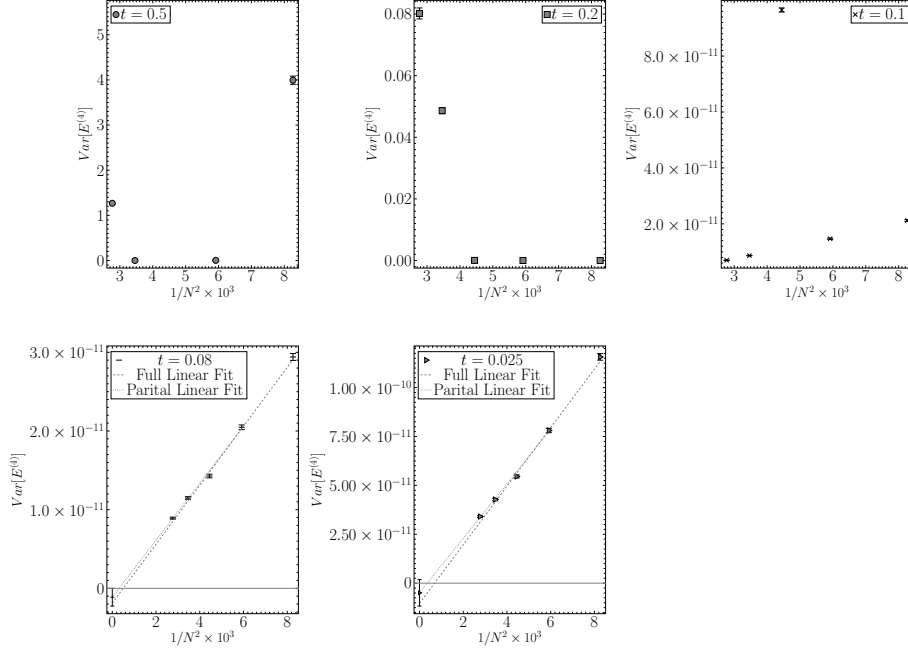
22 *Antonio González-Arroyo, Ken-Ichi Ishikawa, Yingbo Ji, and Masanori Okawa*

Fig. 9. Same as Fig. 8, but for the fourth-order case.

$1/L^2$ dependence and the fit results to the infinite volume limit at $N = 11$ and 19, respectively. The fourth-order coefficients are fitted while the first three order coefficients are fixed to the analytical values. We observed a reasonable χ^2/DoF for the fitting. Table 8 shows the fourth-order coefficients of the PCM in the infinite volume limit at $N = 11$ and 19.

Appendix D. Next-to-leading order coefficient of the TRPCM using analytic method and comparison to NSPT

Analytically, the standard perturbation method is used to calculate the internal energy's next-to-leading order coefficient for the TRPCM. In this appendix, we compare the results between NSPT and the analytic formula in this appendix. The analytic formula for $\langle E^{(2)} \rangle_{\text{ANA}}$ is

$$\langle E^{(2)} \rangle_{\text{ANA}} = E_{\text{planar}}^{(2)} + E_{\text{non-planar}}^{(2)}, \quad (\text{D.1})$$

$$E_{\text{planar}}^{(2)} = \frac{1}{4} \left[\frac{1}{24N^4} \sum_q P(q) - \frac{1}{64} \left(1 - \frac{1}{N^2} \right)^2 \right], \quad (\text{D.2})$$

$$E_{\text{non-planar}}^{(2)} = \frac{1}{16N^4} \sum_p \sum_q P(p)P(q)Q(p,q) \cos \left(\frac{N\bar{K}}{2\pi} (p_1 q_2 - p_2 q_1) \right), \quad (\text{D.3})$$

Perturbative study of large N principal chiral model with twisted reduction 23

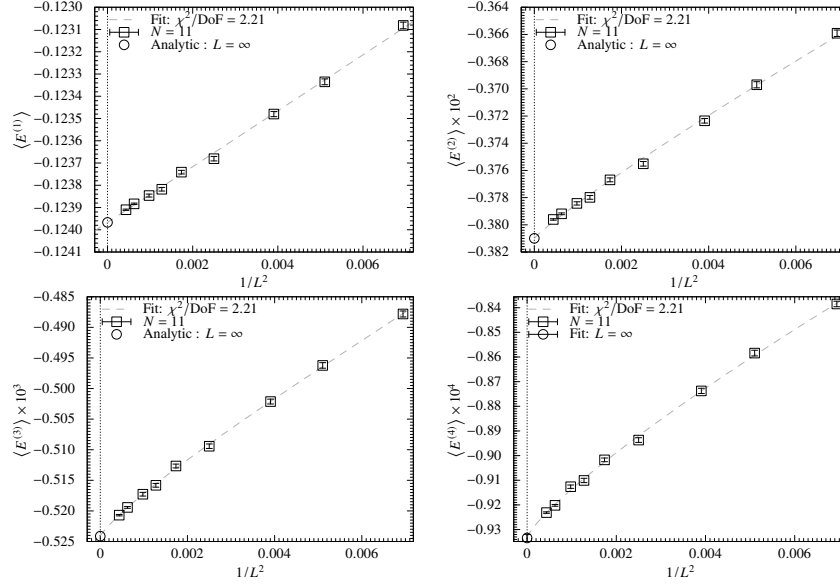


Fig. 10. Volume dependence of $\langle E^{(k)} \rangle$ of the PCM at $N = 11$.

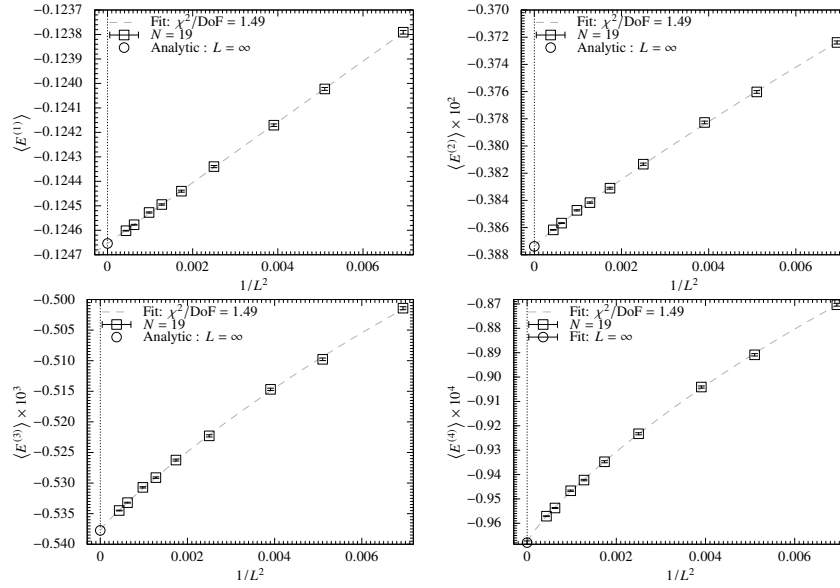


Fig. 11. Volume dependence of $\langle E^{(k)} \rangle$ of the PCM at $N = 19$.

$$P(p) = \frac{1}{2 \sum_{\mu} (1 - \cos(p_{\mu}))}, \quad (\text{D.4})$$

$$Q(p, q) = \sum_{\mu} \left(-\frac{1}{6} + \frac{2}{3} \cos(p_{\mu}) - \frac{1}{2} \cos(p_{\mu} + q_{\mu}) \right). \quad (\text{D.5})$$

24 *Antonio González-Arroyo, Ken-Ichi Ishikawa, Yingbo Ji, and Masanori Okawa*Table 7. Perturbative coefficients of the internal energy for the PCM ($N = 11, 19$).

N	L	$\langle E^{(1)} \rangle$	$\langle E^{(2)} \rangle$	$\langle E^{(3)} \rangle$	$\langle E^{(4)} \rangle$
11	12	-0.123 082(15)	-0.003 659 1(24)	-0.000 487 81(49)	-0.000 083 85(11)
	14	-0.123 335(13)	-0.003 697 0(23)	-0.000 496 22(45)	-0.000 085 84(12)
	16	-0.123 480(12)	-0.003 723 5(17)	-0.000 502 13(40)	-0.000 087 38(11)
	20	-0.123 681(10)	-0.003 755 1(17)	-0.000 509 43(37)	-0.000 089 370(95)
	24	-0.123 741 1(81)	-0.003 766 9(14)	-0.000 512 66(31)	-0.000 090 172(75)
	28	-0.123 817 9(82)	-0.003 779 8(14)	-0.000 515 81(31)	-0.000 091 008(87)
	32	-0.123 846 3(66)	-0.003 784 3(12)	-0.000 517 27(31)	-0.000 091 261(69)
	40	-0.123 883 5(32)	-0.003 791 89(65)	-0.000 519 43(14)	-0.000 092 018(36)
	48	-0.123 910 0(28)	-0.003 796 06(52)	-0.000 520 69(12)	-0.000 092 312(30)
19	12	-0.123 790 8(73)	-0.003 723 9(11)	-0.000 501 42(25)	-0.000 087 032(58)
	14	-0.124 022 4(59)	-0.003 760 25(99)	-0.000 509 77(21)	-0.000 089 087(49)
	16	-0.124 170 6(52)	-0.003 782 70(98)	-0.000 514 68(19)	-0.000 090 409(45)
	20	-0.124 339 7(44)	-0.003 813 38(84)	-0.000 522 28(18)	-0.000 092 326(43)
	24	-0.124 440 2(41)	-0.003 831 04(70)	-0.000 526 24(16)	-0.000 093 475(43)
	28	-0.124 494 7(27)	-0.003 841 64(49)	-0.000 529 11(12)	-0.000 094 226(30)
	32	-0.124 527 3(24)	-0.003 847 33(44)	-0.000 530 70(11)	-0.000 094 664(27)
	40	-0.124 577 3(16)	-0.003 856 74(30)	-0.000 533 202(71)	-0.000 095 372(20)
	48	-0.124 601 7(14)	-0.003 861 68(26)	-0.000 534 485(64)	-0.000 095 708(16)

Table 8. Fourth-order perturbative coefficients of the PCM in the infinite volume limit.

N	$\langle E^{(4)} \rangle$	χ^2/DoF
11	-0.000 093 34(14)	2.21
19	-0.000 096 792(68)	1.49

The primed sum \sum'_p means that $p = 0$ is excluded from the sum and $p_\mu = 2\pi n_\mu/N, n_\mu = 0, \dots, N-1$.

Fig. 12 shows the difference $\langle E^{(2)} \rangle_{\text{NSPT}} - \langle E^{(2)} \rangle_{\text{ANA}}$, where $\langle E^{(2)} \rangle_{\text{NSPT}}$ and $\langle E^{(2)} \rangle_{\text{ANA}}$ are the results with NSPT and standard perturbation theory, respectively. They are consistent within the statistical error.

References

1. S. Profumo, *Journal of High Energy Physics* **2002**, 035 (Oct 2002), doi:10.1088/1126-6708/2002/10/035.
2. L. D. Debbio, H. Panagopoulos, P. Rossi and E. Vicari, *Journal of High Energy Physics* **2002**, 009 (Jan 2002), doi:10.1088/1126-6708/2002/01/009.
3. J. Shigemitsu, J. B. Kogut and D. K. Sinclair, *Phys. Lett. B* **100**, 316 (1981), doi:10.1016/0370-2693(81)90095-2.
4. P. Rossi, M. Campostrini and E. Vicari, *Phys. Rept.* **302**, 143 (1998), arXiv:hep-lat/9609003, doi:10.1016/S0370-1573(98)00003-9.
5. F. Green and S. Samuel, *Nucl. Phys. B* **190**, 113 (1981), doi:10.1016/0550-3213(81)90486-7.
6. E. Abdalla, M. C. B. Abdalla and A. Lima-Santos, *Phys. Lett. B* **140**, 71 (1984), doi:10.1016/0370-2693(84)91050-5, [Erratum: Phys.Lett.B 146, 457–457 (1984)].

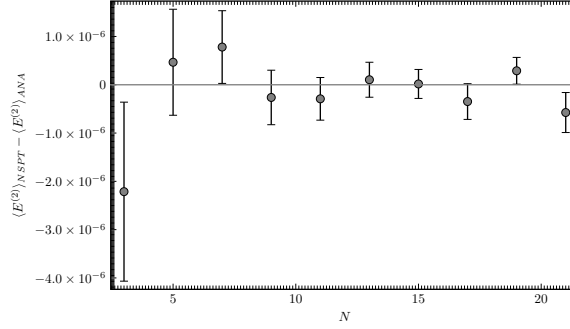


Fig. 12. Difference between $\langle E^{(2)} \rangle_{\text{NSPT}}$ and $\langle E^{(2)} \rangle_{\text{ANA}}$ in next-to-leading order level.

7. P. Wiegmann, *Phys. Lett. B* **142**, 173 (1984), doi:10.1016/0370-2693(84)91256-5.
8. F. Green and S. Samuel, *Phys. Lett. B* **103**, 110 (1981), doi:10.1016/0370-2693(81)90681-X.
9. M. Campostrini, P. Rossi and E. Vicari, *Phys. Rev. D* **52**, 358 (1995), [arXiv:hep-lat/9412098](#), doi:10.1103/PhysRevD.52.358.
10. M. Campostrini, P. Rossi and E. Vicari, *Phys. Rev. D* **52**, 395 (1995), [arXiv:hep-lat/9412102](#), doi:10.1103/PhysRevD.52.395.
11. J. Balog, S. Naik, F. Niedermayer and P. Weisz, *Phys. Rev. Lett.* **69**, 873 (1992), doi:10.1103/PhysRevLett.69.873.
12. G. V. Dunne and M. Unsal, *Phys. Rev. D* **89**, 105009 (2014), [arXiv:1401.5202 \[hep-th\]](#), doi:10.1103/PhysRevD.89.105009.
13. D. Dorigoni, *Annals Phys.* **409**, 167914 (2019), [arXiv:1411.3585 \[hep-th\]](#), doi:10.1016/j.aop.2019.167914.
14. C. Pazarbaşı and D. Van Den Bleeken, *JHEP* **08**, 096 (2019), [arXiv:1906.07198 \[hep-th\]](#), doi:10.1007/JHEP08(2019)096.
15. M. Beneke, *Phys. Rept.* **317**, 1 (1999), [arXiv:hep-ph/9807443](#), doi:10.1016/S0370-1573(98)00130-6.
16. E. Gozzi, C. Pagani and M. Reuter, *Annals Phys.* **429**, 168457 (2021), [arXiv:2004.08874 \[quant-ph\]](#), doi:10.1016/j.aop.2021.168457.
17. F. Di Renzo, G. Marchesini, P. Marenzoni and E. Onofri, *Nucl. Phys. B Proc. Suppl.* **34**, 795 (1994), doi:10.1016/0920-5632(94)90517-7.
18. F. Bruckmann and M. Puhr, *Phys. Rev. D* **101**, 034513 (2020), [arXiv:1906.09471 \[hep-lat\]](#), doi:10.1103/PhysRevD.101.034513.
19. M. Puhr and F. Bruckmann, *PoS LATTICE2018*, 237 (2018), [arXiv:1811.02836 \[hep-lat\]](#), doi:10.22323/1.334.0237.
20. T. Eguchi and H. Kawai, *Phys. Rev. Lett.* **48**, 1063 (1982), doi:10.1103/PhysRevLett.48.1063.
21. G. Bhanot, U. M. Heller and H. Neuberger, *Phys. Lett. B* **113**, 47 (1982), doi:10.1016/0370-2693(82)90106-X.
22. A. González-Arroyo and M. Okawa, *Phys. Lett. B* **120**, 174 (1983), doi:10.1016/0370-2693(83)90647-0.
23. A. González-Arroyo and M. Okawa, *Phys. Rev. D* **27**, 2397 (1983), doi:10.1103/PhysRevD.27.2397.
24. A. González-Arroyo and M. Okawa, *JHEP* **07**, 043 (2010), [arXiv:1005.1981 \[hep-th\]](#), doi:10.1007/JHEP07(2010)043.

26 Antonio González-Arroyo, Ken-Ichi Ishikawa, Yingbo Ji, and Masanori Okawa

25. A. González-Arroyo and M. Okawa, *Nucl. Phys. B* **247**, 104 (1984), doi:10.1016/0550-3213(84)90375-4.
26. A. González-Arroyo and M. Okawa, *JHEP* **06**, 158 (2018), arXiv:1806.01747 [hep-lat], doi:10.1007/JHEP06(2018)158.
27. A. González-Arroyo, I. Kanamori, K.-I. Ishikawa, K. Miyahana, M. Okawa and R. Ueno, *JHEP* **06**, 127 (2019), arXiv:1902.09847 [hep-lat], doi:10.1007/JHEP06(2019)127.
28. G. Parisi and Y.-s. Wu, *Sci. Sin.* **24**, 483 (1981).
29. P. H. Damgaard and H. Huffel, *Phys. Rept.* **152**, 227 (1987), doi:10.1016/0370-1573(87)90144-X.
30. F. Di Renzo, E. Onofri, G. Marchesini and P. Marenzoni, *Nucl. Phys. B* **426**, 675 (1994), arXiv:hep-lat/9405019, doi:10.1016/0550-3213(94)90026-4.
31. M. Brambilla, M. Dalla Brida, F. Di Renzo, D. Hesse and S. Sint, *PoS Lattice2013*, 325 (2014), arXiv:1310.8536 [hep-lat], doi:10.22323/1.187.0325.
32. M. Dalla Brida and D. Hesse, *PoS Lattice2013*, 326 (2014), arXiv:1311.3936 [hep-lat], doi:10.22323/1.187.0326.
33. G. S. Bali, C. Bauer, A. Pineda and C. Torrero, *Phys. Rev. D* **87**, 094517 (2013), arXiv:1303.3279 [hep-lat], doi:10.1103/PhysRevD.87.094517.
34. L. Del Debbio, F. Di Renzo and G. Filaci, *Eur. Phys. J. C* **78**, 974 (2018), arXiv:1807.09518 [hep-lat], doi:10.1140/epjc/s10052-018-6458-9.
35. G. S. Bali, C. Bauer and A. Pineda, *Phys. Rev. D* **89**, 054505 (2014), arXiv:1401.7999 [hep-ph], doi:10.1103/PhysRevD.89.054505.
36. R. Kitano, H. Takaura and S. Hashimoto, *JHEP* **05**, 199 (2021), arXiv:2103.10106 [hep-lat], doi:10.1007/JHEP05(2021)119.
37. M. Dalla Brida, M. Garofalo and A. D. Kennedy, *Phys. Rev. D* **96**, 054502 (2017), arXiv:1703.04406 [hep-lat], doi:10.1103/PhysRevD.96.054502.
38. S. R. Das and J. B. Kogut, *Nucl. Phys. B* **235**, 521 (1984), doi:10.1016/0550-3213(84)90494-2.
39. S. Profumo and E. Vicari, *JHEP* **05**, 014 (2002), arXiv:hep-th/0203155, doi:10.1088/1126-6708/2002/05/014.
40. F. Chamizo and A. González-Arroyo, *J. Phys. A* **50**, 265401 (2017), arXiv:1610.07972 [hep-th], doi:10.1088/1751-8121/aa7346.
41. M. Dalla Brida and M. Lüscher, *Eur. Phys. J. C* **77**, 308 (2017), arXiv:1703.04396 [hep-lat], doi:10.1140/epjc/s10052-017-4839-0.
42. M. Dalla Brida, M. Garofalo and A. D. Kennedy, *Phys. Rev. D* **96**, 054502 (2017), arXiv:1703.04406 [hep-lat], doi:10.1103/PhysRevD.96.054502.
43. P. B. Mackenzie, *Phys. Lett. B* **226**, 369 (1989), doi:10.1016/0370-2693(89)91212-4.
44. A. D. Kennedy and B. Pendleton, *Nucl. Phys. B* **607**, 456 (2001), arXiv:hep-lat/0008020, doi:10.1016/S0550-3213(01)00129-8.
45. P. Rossi and E. Vicari, *Phys. Rev. D* **49**, 6072 (1994), arXiv:hep-lat/9401029, doi:10.1103/PhysRevD.49.6072, [Erratum: Phys.Rev.D 50, 4718 (1994), Erratum: Phys.Rev.D 55, 1698 (1997)].
46. P. Rossi and E. Vicari, *Nucl. Phys. B Proc. Suppl.* **34**, 689 (1994), doi:10.1016/0920-5632(94)90484-7.
47. M. Pühr and F. Bruckmann, *NSPT-scripts* (2019), doi:10.5281/zenodo.3463986.
48. Y. Brihaye and P. Rossi, **235**, 226 (June 1984), doi:10.1016/0550-3213(84)90099-3.
49. Y. Makeenko, *NATO Sci. Ser. C* **556**, 285 (2000), arXiv:hep-th/0001047, doi:10.1007/978-94-011-4303-5_7.
50. B. Lucini and M. Panero, *Phys. Rept.* **526**, 93 (2013), arXiv:1210.4997 [hep-th], doi:10.1016/j.physrep.2013.01.001.

Perturbative study of large N principal chiral model with twisted reduction 27

51. E. Witten, *NATO Sci. Ser. B* **59**, 403 (1980), doi:10.1007/978-1-4684-7571-5_21.